X-ray Absorption Spectroscopy of Mn, Co, Cu, and Zn Inorganic Salts of Tetrathiafulvalene and Bis(ethylenedithio)tetrathiafulvalene

V. Briois,[1a] R. M. Lequan,[1b] M. Lequan,*[,1b] C. Cartier,[1a] G. Van der Laan,[1c] A. Michalowicz,[1d] and M. Verdaguer*[,1a,e]

Laboratoire de Chimie et d'Electrochimie des Matériaux Moléculaires, UA CNRS 429, E.S.P.C.I., 10 rue Vauquelin, 75231 Paris Cedex 05, France; Laboratoire pour l'Utilisation du Rayonnement Electromagnétique (MEN, CEA, CNRS), Université Paris Sud, 91405 Orsay, France; SERC Daresbury Laboratory, Warrington WA4 4AD, United Kingdom; Laboratoire de Physicochimie Structurale, Université Paris-Val de Marne, 94000 Créteil, France; and Laboratoire de Chimie des Métaux de Transition, Université Pierre et Marie Curie, UA CNRS 419, 4 place Jussieu, 75252 Paris Cedex 05, France

Received May 7, 1991. Revised Manuscript Received November 25, 1991

X-ray absorption at the K edges of sulfur, chlorine, and transition-metal ions was investigated for two series of powdered materials: $(TTF)_{14}(MCl_4)_4$ (with M = Mn, Co, and Zn), BEDT-TTF$(MCl_4)_{0.3-0.4}$ (with M = Mn, Co, Cu, and Zn) and in $(TTF)_6(MnCl_3)_3(MnCl_2)_3 \cdot 13H_2O$. From the near-edge absorption fine structures (XANES) and comparison with model compounds, the stereochemistry at the metallic absorbing center is proposed (tetrahedral or distorted tetrahedral for all the MCl_4^{2-} except for the square planar Cu derivative). From the extended absorption fine structures (EXAFS), bond lengths, and Debye-Waller factors around the metallic ions and around the heavy atoms of the inorganic and of the organic species from which the materials are built, are calculated.

Introduction

During the past two decades, a number of "organic metals" based on the organic donor tetrathiafulvalene (TTF[2]) and its derivatives have been reported.[3] At the very beginning, organic acceptors such as tetracyano-*p*-quinodimethane (TCNQ[2]) were combined with TTF derivatives to build donor-acceptor complexes such as TTF-TCNQ.[4] These materials belong to the large family of low-dimensional organic conductors and semiconductors.[5] In these low-dimensional materials, the direction of high electrical conductivity is along the stacks of TTF planar molecules. The short interplanar distances between adjacent molecules (3.39–3.47 Å) allow significant π interactions between the molecular orbitals of the neighbors.[6] The conductivity arises from the migration of π electrons along the stacking axis.

The introduction of metallic counterions in these low-dimensional materials has a more recent history[7] and

Chart I

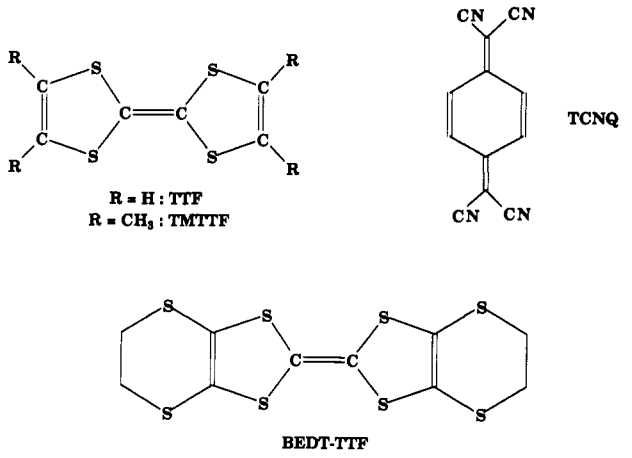

(1) (a) Laboratoire pour l'Utilisation du Rayonnement Electromagnétique (MEN, CEA, CNRS), Université Paris-Sud, 91405 Orsay Cedex, France. (b) Ecole Supérieure de Physique et Chimie Industrielles de Paris, Laboratoire de Chimie et d'Electrochimie des Matériaux Moléculaires, UA CNRS 429, 10 rue Vauquelin, 75231 Paris Cedex 05, France. (c) SERC Daresbury Laboratory, Warrington WA4 4AD, United Kingdom. (d) Laboratoire de Physicochimie Structurale, Université Paris-Val de Marne, 94000 Créteil, France. (e) Laboratoire de Chimie des Métaux de Transition, Université Pierre et Marie Curie, 4 place Jussieu, 75252 Paris Cedex 05, France.

(2) Abbreviations: BEDT-TTF = bis(ethylenedithio)tetrathiafulvalene, EXAFS = extended X-ray absorption fine structure, FT = Fourier transform, TCNQ = tetracyano-*p*-quinodimethane, TMMC = tetramethylammonium manganese trichloride, TMTTF = tetramethyltetrathiafulvalene, TTF = tetrathiafulvalene, XANES = X-ray absorption near-edge structure, XRD = X-ray diffraction.

(3) (a) Cowan, D. O.; Kaufman, J. *J. Am. Chem. Soc.* **1970**, *92*, 219. (b) Scott, B. S.; et al. *J. Am. Chem. Soc.* **1977**, *99*, 6631. (c) Thomas, G. A.; et al. *Phys. Rev. Lett.* **1978**, *41*, 486. (d) Jérome, D.; Mazaud, A.; Ribault, M.; Bechgaard, K. *C. R. Acad. Sci. Paris Ser. B* **1980**, *290*, 27. (e) Teitelbaum, R. C.; et al. *J. Am. Chem. Soc.* **1980**, *102*, 2986. (f) Bechgaard, K.; Carneiro, K.; Olsen, M.; Rasmussen, F. B.; Jacobsen, C. S. *Phys. Rev. Lett.* **1981**, *46*, 852. (g) Saito, G.; Enoki, T.; Toriumi, K.; Inokuchi, H. *Solid State Commun.* **1982**, *42*, 557. (h) Kobayashi, H.; Kato, R.; Mori, T.; Kobayashi, A.; Sasaki, Y.; Saito, G.; Enoki, T.; Inokuchi, H. *Chem. Lett. Chem. Soc. Jpn.* **1984**, 179. (i) Bender, K.; Hennig, I.; Schweitzer, D.; Dietz, K.; Endres, H.; Keller, H. J. *Mol. Cryst. Liq. Cryst.* **1984**, *108*, 359. (j) Papavassiliou, G. C.; Yiannopoulos, S. Y.; Zambounis, J. S. *Mol. Cryst.* **1985**, *120*, 333. (k) Shibaeva, R. P.; Kaminskii, V. F.; Yagubskii, E. B. *Mol. Cryst. Liq. Cryst.* **1985**, *119*, 361. (l) Shaik, S. S.; Whangbo, M.-H. *Inorg. Chem.* **1986**, *25*, 1201. (m) Wang, H. H.; Montgomery, L. K.; Geiser, U.; Porter, L. C.; Carlson, K. D.; Ferraro, J. R.; Williams, J. M.; Cariss, C. S.; Rubinstein, R. L.; Whitworth, J. R.; Evain, M.; Novoa, J. J.; Whangbo, M. H. *Chem. Mat.* **1989**, *1*, 140.

(4) (a) Ferraris, J. P.; Poehler, T. O.; Bloch, A. N.; Cowan, D. O. *Tetrahedron Lett.* **1973**, *27*, 2553. (b) Ferraris, J. P.; Cowan, D. O.; Walatka, V. V. Jr.; Perlstein, J. H. *J. Am. Chem. Soc.* **1973**, *95*, 948. (c) Sandman, D. J. In *Molecular Electronic Devices*; Carter, F. L., Ed.; Marcel Dekker, Inc.: New York; Chapter XI, p 143. (d) Torrance, J. B. *Acc. Chem. Res.* **1979**, *12*, 79. (e) Wudl, F. *Acc. Chem. Res.* **1984**, *17*, 227.

(5) (a) *Low-Dimensional Cooperative Phenomena*; Keller, H. J., Ed.; Plenum Press: New York, 1975. (b) Huizinga, S.; Kommandeur, J.; Sawatzky, G. A.; Kopinga, K.; de Jonge, W. J. M. *Quasi One-Dimensional Conductors*; Ehlers, J., et al., Eds.; Springer: Dubrovnik, 1978; Vol. II, p 45. (c) *Physics in One Dimension*; Bernasconi, J.; Schneider, T., Eds.; Springer: Berlin, 1981. (d) *Organic and Inorganic Low-Dimensional Crystalline Materials*; Delhaes, P., Drillon, M., Eds.; Plenum Press: New York, 1987; Series B: Phys., Vol. 168.

(6) (a) Leung, P. C. W.; Emge, T. J.; Beno, M. A.; Wang, H. H.; Williams, J. M. *J. Am. Chem. Soc.* **1984**, *106*, 7644. (b) Crabtree, G.; Carlson, K. D.; Hall, L. N.; Copps, P. T.; Wang, H. H.; Emge, T. J.; Beno, M. A.; Williams, J. M. *Phys. Rev. B: Condens. Matter* **1984**, *30*, 2958. (c) Williams, J. M.; Emge, T. J.; Wang, H. H.; Beno, M. A.; Copps, P. T.; Hall, L. N.; Carlson, K. D.; Crabtree, G. *Inorg. Chem.* **1984**, *23*, 2558. (d) Cowan, D. O.; Wiygui, F. M. *Chem. Eng. News Special Report* **1986**, *July 21*, 28.

0897-4756/92/2804-0484$03.00/0

created a new area of investigation at the border between organic and inorganic chemistry. The versatility of both chemistries (numerous organic π-donor systems TTF,[2] TMTTF,[2] BEDT-TTF,[2] or π-acceptor TCNQ[2]—whose structures are given in Chart I—against numerous inorganic salts of transition-metals ions) allows one in principle to vary the structure and the electronic and magnetic properties in one or two dimensions.

The structure and the magnetic nature (dia- or paramagnetic) of the inorganic counterions intercalated into the organic lattice are expected to play an important role in the diversity of physical properties of these new "molecular metals".[8]

We present in this paper an X-ray absorption study of three series of compounds for which no or insufficient X-ray diffraction (XRD[2]) structure determination is available and where the conducting properties of the materials preclude obtaining information from visible and ultraviolet electronic spectroscopy.

The aim of this work is 2-fold: first, a characterization of the structure of the counterions introduced in the organic lattice with a determination of the local geometry around the metal and chlorine atoms; second, a description of the interactions between the TTF stacks with a characterization of the local surroundings of the sulfur atoms. We used extended X-ray absorption fine structure (EXAFS) and X-ray absorption near-edge structure (XANES) to obtain structural information about the heavy atoms in the inorganic clusters and in the organic lattice as well.

Experimental Section and Data Analysis

Synthesis. The organometallic complexes of TTF[2] and their derivatives were synthesized as described previously.[7j,8a,9] The crystallization was obtained using the electrooxidation technique. The following salts were prepared: $(TTF)_{14}(MCl_4)_4$ where M = Mn, Co, and Zn;[7j] BEDT-TTF$(MCl_4)_{0.3-0.4}$ where M = Mn, Co, Cu, and Zn;[7k] and $(TTF)_6(MnCl_3)_3(MnCl_2)_3{\cdot}13H_2O$.[8a,9] For clarity, we use simplified formulas instead of the correct stoichiometric one: TTF$(MCl_4)_{0.28}$ instead of $(TTF)_{14}(MCl_4)_4$ and TTF$(MnCl_3)_{0.75}$ instead of $(TTF)_6(MnCl_3)_3(MnCl_2)_3{\cdot}13H_2O$.

The samples used in physical and spectroscopic studies arise from different synthetic batches, but reproducibility of the synthetic procedure was carefully checked (chemical analysis, IR spectroscopy, conductivity, and magnetic properties).

Physical Properties. At room temperature, some of these materials behave like quasi-2D molecular semiconductors. The electric transport and magnetic properties, already published elsewhere, are summarized in Table I: (i) most of the systems are semiconductors except for BEDT-TTF$(CuCl_4)_{0.3}$, which exhibits metallic behavior in the 15–300 K temperature range; (ii) the introduction of a $[Mn^{II}Cl_3]$ unit in the organic mixed-valence compound TTF$(MnCl_3)_{0.75}$ produces a material with a one-dimensional antiferromagnetic behavior.[7j]

Table I. Summary of the Magnetic and Conducting Properties of Materials Studied

	Curie const cm^3 K mol^{-1}	Weiss temp, K	electrical conductivity at room temp, S cm^{-1}	ref
TTF$(MCl_4)_{0.28}$ SERIES				
TTF$(MnCl_4)_{0.28}$	1.09	−4	0.15/SC	7j, 8b
TTF$(CoCl_4)_{0.28}$	0.657	−4	0.15/SC	7j, 8b
TTF$(ZnCl_4)_{0.28}$			0.15/SC	7j, 8b
BEDT-TTF$(MCl_4)_{0.3-0.4}$ SERIES				
BEDT-TTF$(MnCl_4)_{0.3-0.4}$	1.30	−1	0.5/SC	7k
BEDT-TTF$(CoCl_4)_{0.3-0.4}$	0.87	−1.3	0.5/SC	7k
BEDT-TTF$(ZnCl_4)_{0.3-0.4}$	weak Pauli paramagnetism		0.06/SC	7k
BEDT-TTF$(CuCl_4)_{0.3-0.4}$	0.23	−65	50–100/ metallic[a]	7k
TTF$(MnCl_3)_{0.75}$				
TTF$(MnCl_3)_{0.75}$	3.50	−14	15/SC[b]	7j

[a] Metallic behavior at low temperature. [b] Semiconducting behavior at low temperature. SC: semiconductor.

The X-ray absorption characterization has been performed with materials for which the bulk physical properties are reported in Table I.

EXAFS and XANES Measurements. The spectra were measured at room temperature: (i) at the metal K edges (Mn, 6540 eV; Co, 7709 eV; Cu, 8979 eV; Zn, 9659 eV), in transmission mode using ion chambers, at LURE, on the EXAFS III spectrometer, equipped with a double-crystal Si(311) monochromator, with a beam energy of 1.85 GeV and maximum stored current of 300 mA; (ii) at the chlorine (2822 eV) and sulfur (2472 eV) K edges, by collecting the total electron yield, at Daresbury SRS, at the soft EXAFS 3.4 station, equipped with a double-crystal Ge(111) monochromator, with a beam energy of 2 GeV and maximum stored current of 260 mA.

The spectra were recorded with 1-s accumulation time per channel and a stepsize of (i) at the metal K edges, 2 eV for an EXAFS spectrum (1000 eV) and 0.25 eV for a XANES spectrum (100 eV), (ii) at the chlorine and sulfur K edges, 0.5 eV outside the edge region and 0.25 eV at the edge for a XANES spectrum (100 eV), and (iii) at the sulfur K edge, 1 eV for an EXAFS spectrum (500 eV), reduced by chlorine K edge at 2822 eV.

Samples whose spectra were recorded in transmission mode were prepared by depositing thoroughly ground powders between two layers of Kapton adhesive tape. For a surface of 1 cm^2 and a sample mass from 15 to 30 mg, $\Delta\mu x$ is between 0.3 and 1.0 and total $\mu x < 1.5$. Samples whose spectra were recorded by total electron yield were prepared by spreading a suspension in an inert volatile solvent (acetone/alcohol) onto a copper or an aluminium plate.

Data Processing. XANES: For the edge spectra, we subtracted a linear background from the experimental spectrum, by extrapolating the least-squares fitting of the preedge experimental points. As energy reference at the metal K edge, we used the maximum of the first derivative in the metallic foil spectrum, corresponding to the first inflection point in the absorption curve (i.e., 6540 eV for Mn, 7709 eV for Co, 8979 eV for Cu, and 9659 eV for Zn). The energy calibration at the chlorine K edge was chosen arbitrarily at the minimum of the second derivative in the $Ni(en)_3(ClO_4)_2$ complex (2834.5 eV). As an energy calibration for the sulfur K edge, we used the lowest-energy maximum of the first derivative of $MgSO_4$ (2478.5 eV). The spectrum of a thin metallic foil, of $Ni(en)_3(ClO_4)_2$ or of $MgSO_4$, was recorded immediately before and after each XANES spectrum to check the energy calibration. K-edge spectra were normalized by taking the absorbance of the intersection point between the atomic background and the first EXAFS oscillation as unit of absorbance.

(7) (a) Wudl, F.; Ho, C. H.; Nagel, A. *J. Chem. Soc., Chem. Commun.* **1973**, 923. (b) Siedle, A. R.; Candela, G. A.; Finnegan, T. F.; Cape, T.; Hasmall, J. A.; Glick, M.; Ilsley, W. *Ann. N.Y. Acad. Sci.* **1978**, *313*, 377. (c) Aldoshina, M. Z.; Veretennikova, L. S.; Lubovskaya, R. N.; Khidekel, M. L. *Izv. Akad. Nauk. SSSR, SER. Khim.* **1978**, 940. (d) Veretennikova, L. S.; Lubovskaya, R. N.; Lubovskii, R. B.; Rozenberg, L. P.; Simonov, M. A.; Shibaeva, R. P.; Khidekel, M. L. *Dokl. Akad. Nauk. SSSR* **1978**, *241*, 862. (d) Kathirgamanathan, P.; Rosseinsky, D. R. *J. Chem. Soc., Chem. Commun.* **1980**, 356. (f) Batail, P.; Ouahab, I.; Torrance, J. B.; Pylman, M. L.; Parkin, S. S. P. *Solid State Commun.* **1985**, *55*, 597. (g) Miller, J. S.; Krusic, P. J.; Epstein, A. J.; Reiff, W. M.; Zhang, J. H. *Mol. Cryst. Liq. Cryst.* **1985**, *120*, 27. (h) Kawamoto, A.; Tanaka, J.; Tanaka, M. *Acta Crystallogr.* **1987**, *C43*, 205. (i) Geiser, U. *Acta Crystallogr.* **1987**, *C43*, 656. (j) Lequan, M.; Lequan, R. M.; Hauw, C.; Gaultier, J.; Maceno, G.; Delhaes, P. *Synth. Met.* **1987**, *19*, 409. (k) Lequan, M.; Lequan, R. M.; Maceno, G.; Delhaes, P. *J. Chem. Soc., Chem. Commun.* **1988**, 174. (l) Mallah, T.; Hollis, C.; Bott, S.; Day, P.; Kurmoo, M. *Synth. Met.* **1988**, *27*, A38. (m) Penicaud, A.; Batail, P.; Davidson, P.; Levelut, A. M.; Coulon, C.; Perrin, C. *Chem. Mater.* **1990**, *2*, 117.

(8) (a) Lequan, M.; Lequan, R. M.; Delhaes, P. *Tetrahedron Lett.* **1985**, *26*, 5293. (b) Garrigou-Lagrange, Ch.; Rozanski, S.; Kurmoo, M.; Pratt, F. L.; Maceno, G.; Delhaes, P.; Lequan, M.; Lequan, R. M. *Solid State Commun.* **1988**, *67*, 481. (c) Maceno, G.; Garrigou-Lagrange, Ch.; Delhaes, P.; Bechtel, F.; Bravic, G.; Gaultier, J.; Lequan, M.; Lequan, R. M. *Synth. Met.* **1988**, *27*, B5. (d) Maceno, G. Thèse de l'Université de Bordeaux I, 1988. (e) Mallah, T.; Hollis, C.; Bott, S.; Kurmoo, M.; Day, P.; Allan, M.; Friend, R. H. *J. Chem. Soc., Dalton Trans.* **1990**, 859.

(9) Lamache, M.; Kacemi, K. E.; Lequan, M.; Lequan, R. M. *Electrochim. Acta* **1986**, *31*, 499.

Table II. Energy and Absorbance at the Manganese K Edge in the Spectra of $Mn^{II}Cl_4^{2-}$ Derivatives (Figure 1)

sp	compound		pre-edge	edge		1st EXAFS osc
A	$TTF(MnCl_4)_{0.28}$	energy, eV	6541.2 (3)	6549.5 (3)	6552.7 (3)	6570.3 (3)
		abs[a]	0.1	1.51	1.54	1.20
B	$(N(CH_3)_4)_2MnCl_4$ tetrahedron	energy, eV	6541.2 (3)	6551.1 (3)		6570.6 (3)
		abs	0.09	1.58		1.12
C	$(NH_3CH_3)_2MnCl_4$ octahedron	energy, eV	6541.7 (3)	6551.6 (3)		6569.4 (3)
		abs	0.04	1.85		1.14

[a] abs: absorbance.

EXAFS: EXAFS data were processed using the classical plane-wave single scattering[10] approximation, where the EXAFS signal $\chi(k)$ is expressed as a function of the wave vector associated with the ejected photoelectron by a sum of damped sine waves:

$$\chi(k) = S_0^2 \sum_j \left[N_j A_j(k) \exp(-2\sigma_j^2 k^2) \exp\left(\frac{-2R_j}{\lambda(k)}\right) \frac{\sin(2kR_j + \Phi_{ij}(k))}{kR_j^2} \right] \quad (1)$$

where S_0 is a scaling factor, N_j is the number of atoms in the jth scattering shell at a distance R_j from the absorbing atom i, σ_j is the Debye–Waller factor, $\lambda(k)$ is the electron mean free path, approximated in the data processing by $\lambda(k) = k/\Gamma$, where Γ is a fitting parameter, $A_j(k)$ is the amplitude function relative to the jth shell, and $\Phi_{ij}(k)$ is the phase shift relative to the absorbing i and neighboring j pair. At the metal K edge, we either used the amplitude and phase functions tabulated by Teo and Lee[11] or for the manganese compounds the experimental values[12] extracted from the $(N(CH_3)_4)_2MnCl_4$ model.[15] At the sulfur K edge, we used only experimental amplitude and phase functions[12] extracted from the TTF-TCNQ model. When an experimental set of functions was used, the tabulated σ and Γ fitting parameters are relative values with respect to the experimental model. The analysis was performed with a chain of Macintosh microcomputer programs written by one of us.[13]

All EXAFS data were treated in the same way: the preedge region was fitted with a linear and continuous absorption background which was substracted from the total absorption spectrum to give the absorption $\mu(E)$. Then, we fitted the total absorption curve $\mu(E)$ with a smooth "atomic" background absorption $\mu_0(E)$ which, substracted from $\mu(E)$, gives the $\mu(E) - \mu_0(E)$ curve. For the "atomic" background removal we used a polynomial fit of order 5 or 6. The normalized EXAFS signal $\chi(E) = [\mu(E) - \mu_0(E)]/\mu_0(E)$ was transformed in k space ($k^2 = 2m(E - E_0)/h^2$) to obtain $\chi(k)$. The weighted $k^n\chi(k)$ EXAFS signal ($n = 3$ above the metal K edge, $n = 1$ above the sulfur edge) is Fourier transformed to real space, using a Hamming window function with the same range of k.[14] The reliability of the fit is determined by the agreement factor ρ:

$$\rho = \sum_i (\chi_{exp}{}^i(k_i) - \chi_{calc}{}^i(k_i))^2 / \sum_i (\chi_{exp}{}^i(k_i))^2 \quad (2)$$

Results

(1) TTF Derivatives. (1.1) Manganese Derivatives at the Mn K Edge and Cl K Edge (XANES Results). Figure 1 compares the XANES spectrum at the manganese K edge of $TTF(MnCl_4)_{0.28}$ (A) of unknown stereochemical structure with those of two model compounds: the $(N(CH_3)_4)_2MnCl_4$ spectrum (B), where $MnCl_4^{2-}$ is tetrahedral ($Mn-Cl = 2.372$ Å),[15] and the $(NH_3CH_3)_2MnCl_4$ spectrum (C), where Mn has an elongated octahedral surroundings ($Mn-Cl = 2.57$ (2) and 2.51 (2) Å).[16]

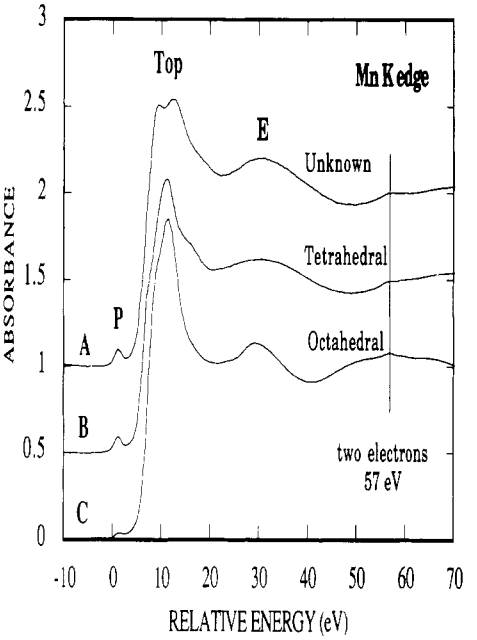

Figure 1. XANES spectra of $TTF(MnCl_4)_{0.28}$ (A), $(N(CH_3)_4)_2MnCl_4$ (B), and $(NH_3CH_3)_2MnCl_4$ (C) at the manganese K edge.

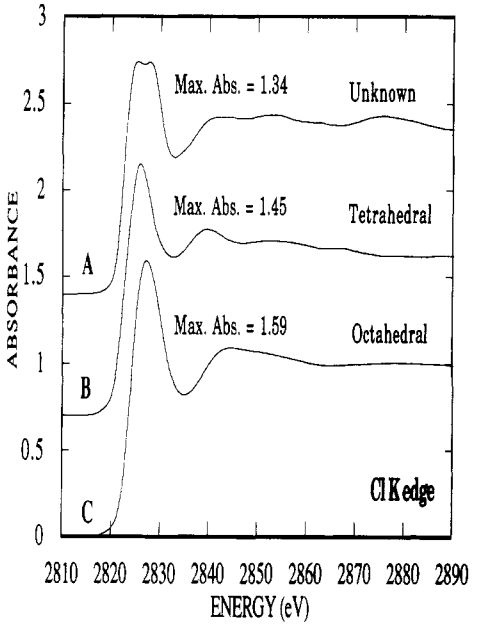

Figure 2. XANES spectra of $TTF(MnCl_4)_{0.28}$ (A), $(N(C_2H_5)_4)_2MnCl_4$ (B), and $(NH_3CH_3)_2MnCl_4$ (C) at the chlorine K edge.

(10) (a) Sayers, D. E.; Stern, E. A.; Lytle, F. W. *Phys. Rev. Lett.* **1971**, *27*, 1204. (b) Kincaid, B. M.; Eisenberger, P. *Phys. Rev. Lett.* **1975**, *34*, 1361. (c) Ashley, C. A.; Doniach, S. *Phys. Rev. B* **1975**, *11*, 1279. (d) Lee, P. A.; Pendry, J. B. *Phys. Rev. B* **1975**, *11*, 2795. (e) Teo, B. K. *EXAFS: Basic Principles and Data Analysis*; Springer Verlag: Berlin, 1986.

(11) Teo, B. K.; Lee, P. A. *J. Am. Chem. Soc.* **1979**, *101*, 2815.

(12) (a) Lee, P. A.; Beni, G. *Phys. Rev. B* **1977**, *15*, 2862. (b) Stern, E. A.; Bunker, B. A.; Heald, S. M. *Phys. Rev. B* **1980**, *21*, 5521.

(13) Michalowicz, A. *EXAFS pour le MAC, Logiciels pour la chimie*; Société Française de Chimie: Paris, 1991; pp 102–103.

(14) (a) *EXAFS Spectroscopy, Techniques and Applications*; Teo, B. K., Joy, D. C., Eds.; Plenum: New York, 1981. (b) Cramer, S. P.; Hodgon, K. O. *Prog. Inorg. Chem.* **1979**, *25*, 1. (c) Lee, P. A.; Citrin, P. H.; Eisenberger, P.; Kincaid, B. M. *Rev. Mod. Phys.* **1981**, *53*, 769.

(15) Wiesner, J. R.; Srivastava, R. C.; Kennard, C. H. L.; Vaira, M. D.; Lingafelter, E. C. *Acta Crystallogr.* **1967**, *23*, 565.

(16) (a) Kind, R.; Roos, J. *Phys. Rev. B* **1976**, *13*, 45. (b) Heger, G.; Mullen, D. M.; Knorr, K. *Phys. Status Solidi* **1975**, *31*, 455. (c) Heger, G.; Mullen, D. M.; Knorr, K. *Phys. Status Solidi* **1976**, *35*, 627.

Table III. Energy and Absorbance in the Spectra of $M^{II}Cl_4^{2-}$ Derivatives at the Metal K Edges (Figure 3) and at the Chlorine K Edge (Figure 4)

			Metal K edge					
				edge			chloride K edge	
sp	$TTF(MCl_4)_{0.28}$		pre-edge			1st EXAFS osc		
A	Mn	energy, eV	6541.2 (3)	6549.5 (3)	6552.7 (3)	6570.3 (3)	2825.2 (3)	2827.7 (3)
		abs[a]	0.1	1.51	1.54	1.20	1.51	1.54
B	Co	energy, eV	7709.2 (3)	7722.3 (3)		7742.2 (3)	2825.7 (3)	
		abs	0.06	1.35		1.11	1.44	
C	Zn	energy, eV		9664.1 (3)		9685.2 (3)	2825.2 (3)	
		abs		1.68		1.08	1.44	

[a] abs: absorbance.

The energy values and relative intensity of the main spectral features are displayed in Table II.

The spectrum of $(NH_3CH_3)_2MnCl_4$ (C) shows a main peak of high intensity, a weak preedge, which is usual in octahedral complexes.[17] The edge spectrum of $TTF(MnCl_4)_{0.28}$ (A) is different from that of $(NH_3CH_3)_2MnCl_4$ (C) but resembles that of $(N(CH_3)_4)_2MnCl_4$ (B): the intensity and energy of their preedge P are identical, the intensities of the main peak of their edge are almost equal. The first EXAFS oscillation (E) in both spectra coincides. The main difference between (A) and (B) is the splitting in the edge (A); the energies of the two main peaks point at ±1.6 eV from the energy of the main edge transition in (B). In all the spectra (A)–(C) a weak absorption band is located at 57 eV above the preedge structure.

Figure 2 shows the chlorine K XANES spectrum of $TTF(MnCl_4)_{0.28}$ (A) together with the tetrahedral model compound $(N(C_2H_5)_4)_2MnCl_4$ (B) and with the octahedral one $(NH_3CH_3)_2MnCl_4$ (C). The relative intensities of the main edge are indicated on the figure. Similar to the metal K edge, the chlorine edge of $(NH_3CH_3)_2MnCl_4$ (C) shows an intense main peak compared to $TTF(MnCl_4)_{0.28}$ (A) and $(N(C_2H_5)_4)_2MnCl_4$ (B). $TTF(MnCl_4)_{0.28}$ (A) also shows a splitting of the edge with peaks at 2825.3 and 2827.7 eV.

(1.2) $TTF(MCl_4)_{0.28}$ (M = Mn, Co, Zn) at the Metal K Edge, Cl K Edge and S K Edge. XANES results: The experimental data for the compounds (M = Mn, Co, and Zn) in this series are shown in Figure 3 for the metal K edge and in Figure 4 for the chlorine K edge: (A) $TTF(MnCl_4)_{0.28}$, (B) $TTF(CoCl_4)_{0.28}$, and (C) $TTF(ZnCl_4)_{0.28}$. A relative energy scale is used at the metal K edge. Table III summarizes the energy and absorbance values in the series at both edges.

At the metal edge, the spectra are similar, except that the intensity of the preedge is decreasing going from the manganese to the cobalt compound with complete quenching for the zinc compound.

At the chlorine K edge, the similarity between the three spectra is even more striking, in particular for the spectrum (B) of $TTF(CoCl_4)_{0.28}$ and (C) of $TTF(ZnCl_4)_{0.28}$, which are completely superimposable.

The XANES spectra at the sulfur K edge of the $TTF(MnCl_4)_{0.28}$ series are given in Figure S1.[28] The three spectra are very similar (same energies and same intensities of the white lines in particular) and, as in the chlorine K edge, the spectra of $TTF(CoCl_4)_{0.28}$ and $TTF(ZnCl_4)_{0.28}$ are the same. The XANES spectrum of $TTF(CoCl_4)_{0.28}$ (A) is shown in Figure 5 together with TTF-TCNQ[18b,c] (B) and

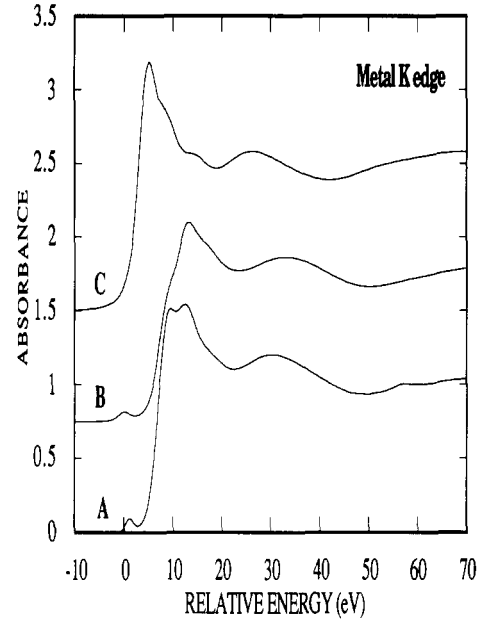

Figure 3. XANES spectra of $TTF(MCl_4)_{0.28}$ where M = Mn (A), Co (B), and Zn (C) at the metal K edges. The value of zero energy is 6540 eV for (A), 7709 eV for (B), and 9659 eV for (C).

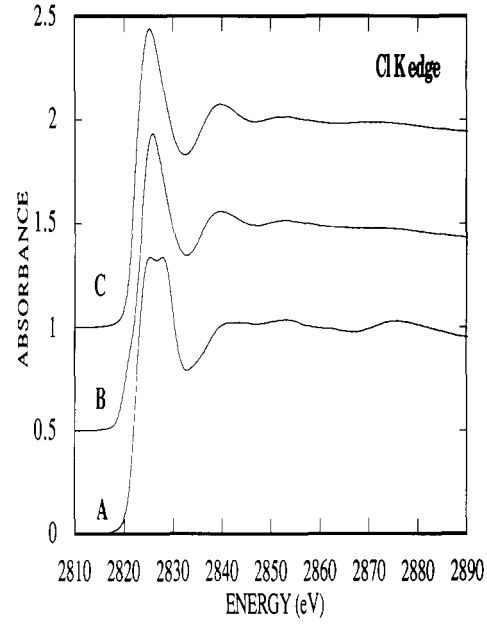

Figure 4. XANES spectra of $TTF(MCl_4)_{0.28}$ where M = Mn (A), Co (B), and Zn (C) at the chlorine K edge.

TTF[18a,c] (C) models. The spectrum of $TTF(CoCl_4)_{0.28}$ does resemble that of TTF-TCNQ more than that of TTF above the main edge. But the spectra of the $TTF(MCl_4)_{0.28}$ series differ from those of TTF and TTF-TCNQ in the shape of the main edge: indeed, there is a clear shoulder on this

(17) (a) Cartier, C. Thèse de l'Université Paris-Sud, 1988. (b) Benfatto, M.; Natoli, C. R.; Garcia, J.; Bianconi, A. *J. Phys.* **1986**, *47*, C8, 25. (c) Garcia, J.; Bianconi, A.; Benfatto, M.; Natoli, C. R. *J. Phys.* **1986**, *47*, C8, 49.

(18) (a) Cooper, W. F.; Kenny, N. C.; Edmonds, J. W.; Nagel, A.; Wudl, F.; Coppens, P. *J. Chem. Soc., Chem. Commun.* **1971**, 889. (b) Phillips, T. E.; Kistenmacher, T. J.; Ferraris, J. P.; Cowan, D. O. *J. Chem. Soc., Chem. Commun.* **1973**, 471. (c) Kistenmacher, T. J.; Phillips, T. E.; Cowan, D. O. *Acta Crystallogr.* **1974**, *B30*, 763.

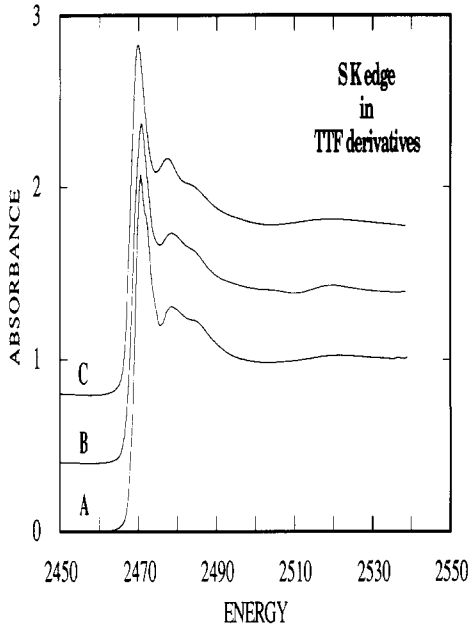

Figure 5. XANES spectra of $TTF(CoCl_4)_{0.28}$ (A), TTF-TCNQ (B), and TTF (C) at the sulfur K edge.

Table IV. EXAFS Results at the Metal K Edge in the TTF Derivatives

$TTF(MCl_4)_{0.28}$	N	σ, Å	R, Å	$\Gamma = k/\lambda$	E_0, eV	ρ, %
Mn[a]	4	0.08	2.35 (2)	0.4	6551	0.3
Mn[b]	4	0.03	2.36 (2)	0.4	6546	0.3
Co[a]	4	0.07	2.26 (2)	0.6	7724	0.6
Zn[a]	4	0.08	2.26 (2)	0.4	9689	0.4

[a] With tabulated values of Teo and Lee.[11] [b] With experimental parameters.

peak. The main difference appears between the spectrum of TTF and the two other ones: the white line is shifted to higher energy in the partially oxidized compounds, and so are the EXAFS oscillations.

EXAFS results at the metal K edge: the spectra and their Fourier transforms are very similar, at all edges. One of them is presented in the supplementary material: (i) the EXAFS spectrum $\chi(k)$ of the Mn complex $TTF(MnCl_4)_{0.28}$, in Figure S2;[28] (ii) the corresponding $k^3\chi(k)$ Fourier transform (FT^2) in Figure S3;[28] (iii) the filtered first-shell experimental spectrum and the simulated EXAFS spectrum are shown in Figure S4.[28]

The Fourier transform of the $TTF(MnCl_4)_{0.28}$ compound shows only a single peak corresponding to the Cl shell. The results of the best fit for each compound are given in Table IV.

We used the theoretical phase and amplitude functions given by Teo and Lee[11] and the experimental values for the manganese compound. All results were obtained in a k range from 3.8 to 11 $Å^{-1}$.

EXAFS results at the sulfur K edge: the Fourier transforms of the EXAFS signal above the S-K edge for the three compounds of the $TTF(MCl_4)_{0.28}$ series are very similar. Only the result for $TTF(CoCl_4)_{0.28}$ is presented and compared to those of TTF[18a,c] and TTF-TCNQ.[18b,c] The EXAFS signals of TTF, TTF-TCNQ, and $TTF(CoCl_4)_{0.28}$ are shown in Figure 6. The corresponding k^1-weighted Fourier transforms are given in Figure 7. The k range used is the same for the three compounds, 2.7–9.0 $Å^{-1}$, since the analysis is limited due to the energy position of the chlorine K edge (≈350 eV above the sulfur edge) encountered in the $TTF(MCl_4)_{0.28}$ series. The Fourier transforms of TTF, TTF-TCNQ, and $TTF(CoCl_4)_{0.28}$ are

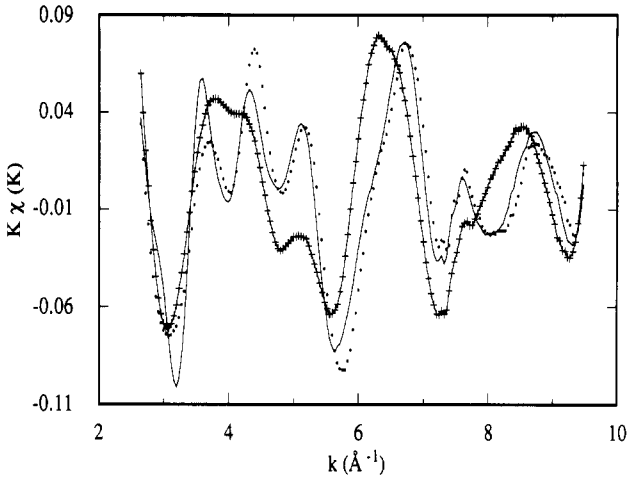

Figure 6. EXAFS signals of TTF (+) TTF-TCNQ (—), and $TTF(CoCl_4)_{0.28}$ (···) (S K edge).

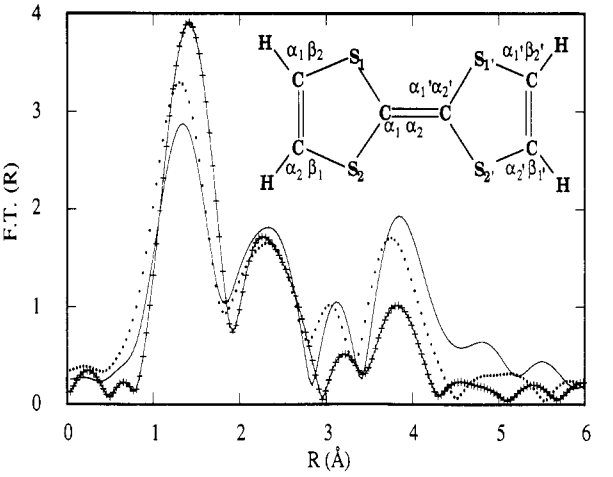

Figure 7. Fourier transforms of TTF (+), TTF-TCNQ (—), and $TTF(CoCl_4)_{0.28}$ (···) (S K edge).

Table V. EXAFS Results at the Sulfur K Edge

compound	N	σ, Å	R, Å	$\Gamma = k/\lambda$	E_0, eV	ρ, %	nature
			Shell 1				
TTF-TCNQ[18c]	2		1.74		2482		S–C_α
TTF	2	−0.004	1.74 (2)	−0.17	2471	6.3	
$TTF(CoCl_4)_{0.28}$	2	0.033	1.72 (2)	−0.24	2484	4.0	
			Shell 2				
TTF-TCNQ[18c]	1		2.62		2482		S–C_β
TTF	1	≈0.0	2.63 (2)	0.09	2481	0.2	
$TTF(CoCl_4)_{0.28}$	1	0.027	2.61 (2)	0.07	2484	0.5	
			Shell 3				
TTF-TCNQ[18c]	2		3.47		2482		S–S_{int}
TTF	1.24	0.036	3.60 (2)	−0.03	2488	0.8	
$TTF(CoCl_4)_{0.28}$	1.33	≈0.0	3.42 (2)	−0.04	2477	0.5	

composed of three clearly resolved peaks, at ≈1.3–1.4 Å, ≈2.3–2.4 Å and ≈3.0–3.2 Å (without phase shift correction) which can be assigned to intramolecular S-C_α, S-C_β, and intermolecular S–S distances, respectively, shown in scheme inserted in Figure 7. The fourth peak (at ≈3.8 Å), which can be assigned in TTF to the S_1–S_1' and S_2–S_2' intramolecular distance, cannot be assigned so simply in TTF-TCNQ and $TTF(CoCl_4)_{0.28}$ since there are several contributions.

We used the experimental phase and amplitude functions extracted from the TTF-TCNQ model to fit the inverse filtered Fourier transforms of the first three shells. The results are given in Table V. The results for the third

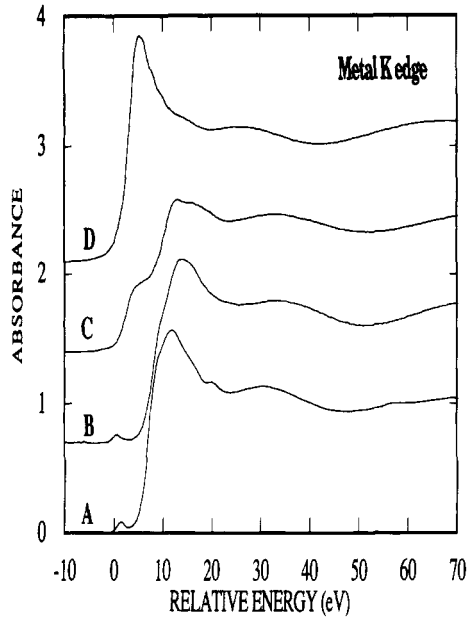

Figure 8. XANES spectra of BEDT-TTF$(MCl_4)_{0.3-0.4}$, M = Mn (A), Co (B), Cu (C), and Zn (D) at the metal K edges. The value of zero energy is 6540 eV for (A), 7709 eV for (B), 8979 eV for (C), and 9659 eV for (D).

Table VI. Energy and Absorbance in the Spectra of $M^{II}Cl_4^{2-}$ Derivatives at the Metal K Edges (Figure 8)

sp	BEDT-TTF$(MCl_4)_{0.3}$		preedge	edge	1st EXAFS osc
A	Mn	energy, eV	6541.4 (3)	6552.0 (3)	6570.5 (3)
		abs[a]	0.09	1.57	1.14
B	Co	energy, eV	7709.7 (3)	7724.8 (3)	7742.6 (3)
		abs	0.07	1.42	1.10
D	Zn	energy, eV		9664.7 (3)	9683.8 (3)
		abs		1.72	1.05

[a] abs: absorbance.

shell result from a fitting of the inverse filtered Fourier transform of the second and third shell together, where the parameters of the second shell were kept constant.

(2) BEDT-TTF Derivatives. These compounds were investigated at the metal K edges only. **XANES results:** The spectra of the series BEDT-TTF$(MCl_4)_{0.3}$, where M = Mn, Co, Zn, and Cu, are presented in Figure 8 with a relative energy scale: (A) Mn, (B) Co, (C) Zn, and (D) Cu. The spectrum of BEDT-TTF$(CoCl_4)_{0.3}$ was recorded on the dispersive EXAFS spectrometer, with Si(311) crystals.

We have the same absorption bands in this series as in the preceding one. Nevertheless, the manganese compound does not have a split main peak. The spectrum of the copper compound shows a pre-edge of weak intensity and a well-defined shoulder in the leading edge.

The values of the energy and absorbance of the main features in the spectra are presented in Table VI.

EXAFS results: The EXAFS signal of the cobalt complex BEDT-TTF$(CoCl_4)_{0.3}$ is displayed in Figure S5;[28] the corresponding inverse filtered Fourier transform for the first shell, superimposed with the best theoretical fit curve, is shown in Figure S6.[28] Table VII summarizes our fitting results for the series, obtained with Teo and Lee's phase and amplitude parameters.[11]

The fit was done with a single-shell fitting procedure in the k-space range 3.8–10.5 $Å^{-1}$.

(3) TTF$(MnCl_3)_{0.75}$. We investigated the Mn and the Cl K edges.

Table VII. EXAFS Results at the Metallic Edge for the BEDT-TTF Derivatives

BEDT-TTF$(MCl_4)_{0.3}$	N	σ, Å	R, Å	$\Gamma = k/\lambda$	E_0, eV	ρ, %
Mn	4	0.10	2.35 (2)	0.5	6551	1.8
Co	4	0.09	2.26 (2)	0.5	7723	0.7
Zn	4	0.09	2.24 (2)	0.3	9688	0.5

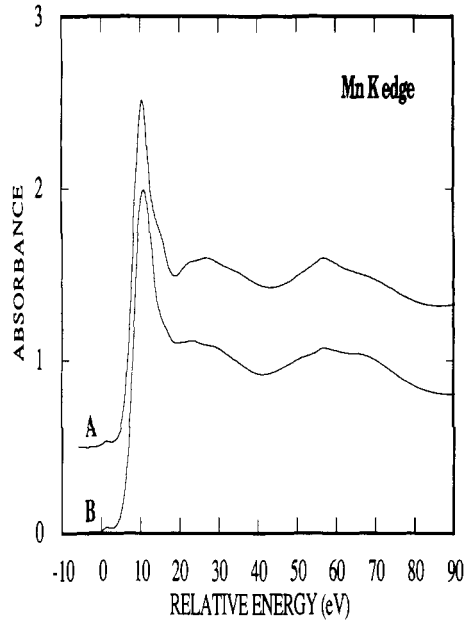

Figure 9. K-edge absorption spectrum of manganese in $(N(CH_3)_4)MnCl_3$ or TMMC (A) and TTF$(MnCl_3)_{0.75}$ (B).

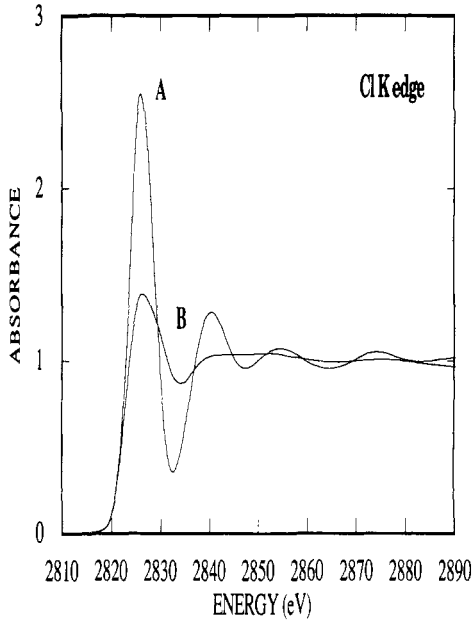

Figure 10. K-edge absorption spectrum of chlorine in $(N(CH_3)_4)MnCl_3$ or TMMC (A) and TTF$(MnCl_3)_{0.75}$ (B).

XANES results: The experimental spectra at the manganese K edge of an octahedral model compound, tetramethylammonium manganese trichloride $(N(CH_3)_4)MnCl_3$ (TMMC),[19] (A) and of TTF$(MnCl_3)_{0.75}$ (B) are shown in Figure 9.

The spectra are similar but not completely equal. They display a weak-intensity preedge transition and an intense main edge.

The chlorine K XANES spectra of both TMMC (A) and TTF$(MnCl_3)_{0.75}$ (B) are presented in Figure 10. Contrary

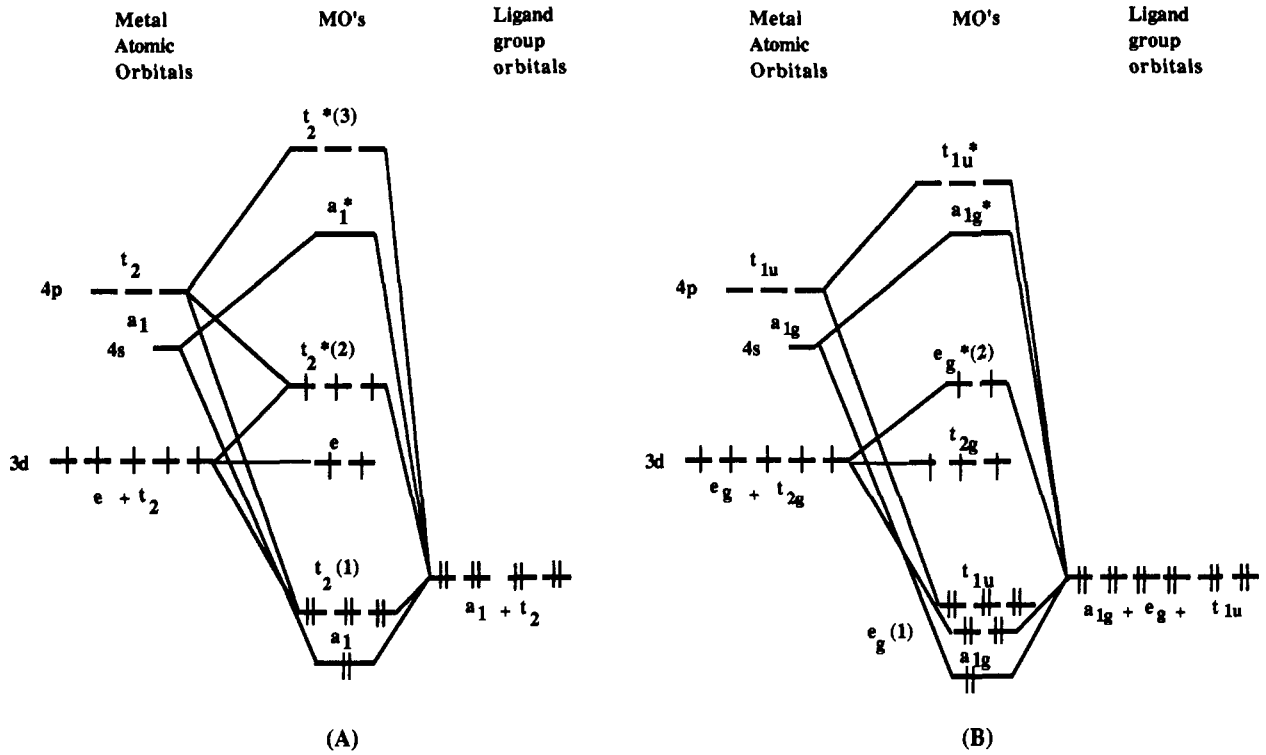

Figure 11. Schematic molecular orbitals energy diagrams for a tetrahedral complex (A) and for an octahedral complex (B). π bonding is not included. The 3d orbitals occupancy shown is for Mn(II), d^5.

Table VIII. Energy and Absorbance for the Spectra at the Manganese K Edge in Figure 9 and the Chlorine K Edge in Figure 10

sp	compound		manganese K edge: pre-edge	manganese K edge: edge	chlorine K edge
A	TMMC distorted octahedron	energy, eV	6541.3 (3)	6550.3 (3)	2826.0 (3)
		abs	0.04	2.04	2.55
B	$TTF(MnCl_3)_{0.75}$	energy, eV	6541.4 (3)	6550.7 (3)	2826.2 (3)
		abs	0.04	2.00	1.39

to those at the metal K edge, they are very different. The TMMC spectrum shows an intense main edge and clear EXAFS oscillations, whereas the $TTF(MnCl_3)_{0.75}$ spectrum has a weak intensity at the edge and weak EXAFS oscillations.

The values of the energy and absorbance of the main features for both edges are presented in Table VIII.

EXAFS results: Figure S7[28] gives the experimental EXAFS signal $\chi(k)$, whereas Figure S8[28] shows the $k^3\chi(k)$ FT in the real R space. The FT presents two peaks at ≈2.1 and 3.0 Å (without phase correction) assigned respectively to the Mn–ligand distances in the first coordination shell and to Mn–Mn distances. Figures S9 and S10[28] display the filtered EXAFS spectrum $k^3\chi(k)$ vs k and the best fit for the first and second peaks respectively.

Table IX gives the results of the best fits using Teo and Lee's[11] phase and amplitude functions. The k range is 3.8–1.04 $Å^{-1}$. We used a three-neighbors fitting procedure for the first shell: two different Mn–Cl shells, one Mn–O. We used a single neighbor procedure for the second shell.

Discussion

We discuss for each series of compounds the XANES and EXAFS results for the inorganic anion. In case of the TTF derivatives, we complete the description of the structure with EXAFS results on the organic lattice.

(1) TTF Derivatives. (A) Characterization of the Geometry of the Inorganic Moiety. XANES analysis:

Table IX. EXAFS Results at the Mn Edge for the $TTF(MnCl_3)_{0.75}$

shell	N	σ, Å	R, Å	$\Gamma = k/\lambda$	E_0, eV	ρ, %
			Shell 1			
Mn–Cl	4	0.12	2.49 (2)	0.7	6552	1.0
Mn–Cl	0.5	0.06	2.55 (2)	0.7	6552	1.0
Mn–O	1.5	0.13	2.05 (2)	0.7	6533	1.0
			Shell 2			
Mn–Mn	2	0.15	3.28 (2)	0.3	6560	1.6

(i) The spectrum at the manganese K edge of $(N(C_2H_5)_4)_2MnCl_4$ (Figure 1B) corresponds to a distorted tetrahedron,[15] whereas the spectrum of $(NH_3CH_3)_2MnCl_4$ (Figure 1C) is characteristic of a distorted octahedron.[16]

Pre-edge. In this energy range, which corresponds to transitions to bound states, the features can be interpreted, assuming a molecular orbital (MO) scheme, as electric dipole transitions of the photoelectron from the 1s level to an excited state, implying the first singly occupied MO of the 3d and 4p atomic orbitals of the metal (M(3d), M(4p)) and of the 3p orbitals of the chloro ligand (L(3p)).

For a given d^n configuration, an intense preedge is found in complexes without an inversion center, as in tetrahedral symmetry. In a T_d point group (see Figure 11), electric dipole transitions to molecular levels t_2*(2) are allowed. On the contrary, in complexes with an inversion center, such as an octahedron, selection rules forbid the transition from 1s to t_{2g} and e_g MOs; consequently, the pre-edge is weak and partly takes its intensity from quadrupole transition.[20]

These features are clearly observed in the spectra of our model compounds.

Edge. The intensity of the main peak (the so-called "white line") in the octahedral spectrum is larger than in

(19) (a) Morosin, B.; Graeber, E. J. *Acta Crystallogr.* **1967**, *23*, 766. (b) Dupas, C.; Clément, S.; Verdaguer, M., work in progress.

(20) Hahn, J. E.; Scott, R. A.; Hodgson, K. O.; Doniach, S.; Desjardins, S.; Solomon, E. I. *Chem. Phys. Lett.* **1982**, *88*, 595.

the tetrahedral. This peak is firmly established as a transition of the 1s electron to a p symmetry empty state. Earlier we proposed[21] that the decrease of the intensity of the main edge in tetrahedral complexes compared to the octahedral ones is related to a reduced participation of the 4p AOs of the metal in the t_2*(3) orbital: in the tetrahedron, there is an increased overlap between the metal and ligand orbitals due to the shorter distance, hence an increased ligand participation in the t_2*(3). There is also some mixing of the 3d AOs of the metal in the molecular t_2*(3) orbital. The correlated mixing of 4p–3d metallic orbitals, in the molecular t_2*(2) orbital gives rise to the enhanced intensity of the preedge in the tetrahedral complexes.

The first EXAFS oscillation in the octahedral spectrum is at lower energy than in the tetrahedral. This is expected from the larger metal–ligand distances in the octahedron (2.57 (2) and 2.51 (2) Å)[16] than in the tetrahedron (2.372 Å).[15]

The weak absorption band at 57 eV appears independent of the structure of the complex. We associate this feature with a two-electron transition.

The description and interpretation of XANES spectra at the chlorine K edge are less evolved in the literature[22] than those at the metal K edges, but a similar analysis in terms of the local symmetry around the chlorine is possible and converges with the interpretation formulated by Sugiura et al.[22a] and Hedman et al.[22d] The transitions involved in the spectra of the tetrahedral $(N(C_2H_5)_4)_2MnCl_4$ and octahedral $(NH_3CH_3)_2MnCl_4$ model compounds at the chlorine K edge are essentially atomic-like. In C_{3v} symmetry ($(N(C_2H_5)_4)_2MnCl_4$) or in C_{4v} symmetry ($(NH_3CH_3)_2MnCl_4$), the main-edge transition in both spectra (Figure 2) is an allowed transition of the Cl(1s) electron to the Cl(4p) unoccupied level. Although the Cl(4s) level is the lowest unoccupied one, the 1s → 4s transition is not electric dipole allowed. The intensity of the main peak for the octahedral model compound (C) is higher than for the tetrahedral one (B). The interpretation is the same as for the metal K edge. The mixing of the Cl(4p) atomic orbitals with the M(4p) ones in molecular levels of the proper symmetry is larger in the tetrahedral model compound than in the octahedral one due to shorter Cl–Mn distances in the tetrahedron. Less Cl(4p) orbitals are locally available in the tetrahedral model; hence, there is a weaker intensity of the main edge in the tetrahedron.

(ii) The local environment of Mn in $TTF(MnCl_4)_{0.28}$ can now be determined by a simple comparison between the spectra at the metal and chlorine K edges of $(NH_3CH_3)_2MnCl_4$ (symmetry O_h) and $(N(CH_3)_4)_2MnCl_4$ (symmetry T_d): the manganese appears to be in a tetrahedral environment in $TTF(MnCl_4)_{0.28}$.

The splitting of the main peak of $TTF(MnCl_4)_{0.28}$ at the metal K edge is attributed to a splitting of the Mn 4p(t_2) orbitals. It can arise from two origins: either different Mn–Cl distances, or different Cl–Mn–Cl angles. As EXAFS suggests an uniform distance (Mn^{II}–Cl = 2.36 Å, σ = 0.08 Å), the presence of different Cl–Mn–Cl angles is the most probable situation.

The same peak splitting is encountered in the Cl K edge spectrum. The Cl(4p) orbitals are equally split into two orbital groups because of the distortion of the structure.

(21) Briois, V.; Cartier, C.; Momenteau, M.; Maillard, Ph.; Zarembowitch, J.; Dartyge, E.; Fontaine, A.; Tourillon, G. Thuéry, P.; Verdaguer, M. *J. Chim. Phys.* **1989**, *86*, 1623.

(22) (a) Sugiura, C.; Suzuki, T. *J. Chem. Phys.* **1981**, *75*, 4357. (b) Sugiura, C. *J. Chem. Phys.* **1973**, *58*, 5444. (c) Bhat, N. V. *Spectrochim. Acta* **1973**, *28B*, 257. (d) Hedman, B.; Hodgson, K. O.; Solomon, E. I. *J. Am. Chem. Soc.* **1990**, *112*, 1643.

Table X. Correlation between Preedge Intensity and 3d Orbitals Occupancy

M(II)	electronic structure		pre-edge abs	pre-edge energy, eV
Mn	$3d^5$	t_2 ↑ ↑ ↑ e ↑ ↑	0.09	6541.2
Co	$3d^7$	t_2 ↑↓ ↑ ↑ e ↑↓ ↑↓	0.06	7709.2
Zn	$3d^{10}$	t_2 ↑↓ ↑↓ ↑↓ e ↑↓ ↑↓	0.00	

Table XI. Comparison between M–Cl Distances (Å) Determined by EXAFS and XRD

metal	$TTF(MCl_4)_{0.28}$ EXAFS	$TTF(MCl_4)_{0.28}$ XRD	tetrahedral models XRD
Mn	2.35 (2)	unknown	2.372[15] 2.280[15]
Co	2.26 (2)	2.263/2.278/2.251 2.251 ± 0.02[24]	2.252 (13)[23a] 2.2505 (55)[25]
Zn	2.26 (2)	unknown	2.287[15]

(iii) In this third section, we discuss the evolution of the spectra when changing the metal (Figure 3 and 4).

In the case of $TTF(CoCl_4)_{0.28}$, our data confirm the XRD structure;[8d] the inorganic anion $CoCl_4^{2-}$ is a tetrahedron, as also is $ZnCl_4^{2-}$.

The structural distortion, discussed above, seems to decrease from the manganese to the zinc: in Figure 3, there are two main peaks for $TTF(MnCl_4)_{0.28}$, one shoulder in the rising edge and one main peak for $TTF(CoCl_4)_{0.28}$. We conclude that the zinc compound is the most regular tetrahedron in the series, the manganese compound is the most distorted one with respect to the tetrahedron, and the cobalt compound is an intermediate case.

If we compare the preedge in the metal K edge spectra for the TTF series, we observe a decrease in intensity from Mn(II) to Zn(II) spectra. Everything being equal, the intensity of the preedge probes the number of unoccupied d states in the transition metal. The transition intensity is proportional to the number of empty states: the intensity decreases going from the half-occupied d^5 configuration of Mn(II) to the d^7 (Co(II)) and the totally occupied d^{10} (Zn(II)) configuration (see Table X).

The apparent relative shift of the leading edge of $TTF(ZnCl_4)_{0.28}$ to lower energy with respect to $TTF(MCl_4)_{0.28}$ (M = Mn and Co) can be explained by the fact that the value of zero energy (which is the Fermi level of the metal) corresponds to 3d empty levels in metallic manganese and cobalt, whereas in metallic zinc it corresponds to 4p empty levels at higher energy.

At the chlorine K edge (Figure 4), the spectra of $TTF(CoCl_4)_{0.28}$ and $TTF(ZnCl_4)_{0.28}$ are very similar in shape, intensity, and energy position. The region above the XANES is the same in both spectra: the structure of the MCl_4 entity and the Cl–M distances are similar in both compounds. The splitting of the main edge in $TTF(MnCl_4)_{0.28}$ confirms the distortion of the anion.

EXAFS analysis: The EXAFS analysis at the metal K edge gives M–Cl distances which are comparable to those in the literature (Table XI). Within the error bars of our EXAFS results, the distances obtained by XAS and XRD can be considered to be equal.

The M–Cl distances for the cobalt and zinc compounds are almost equal.

(B) Structural Characterization of the Organic Lattice. XANES analysis: The shift to higher energy of the white line (≈0.7 eV) in the two partially oxidized compounds $TTF(CoCl_4)_{0.28}$ and TTF–TCNQ[18b,c] compared to TTF[18a,c] (Figure 5) is a clear indication that the charge-transfer affects the sulfur atoms and that *the sulfur itself is partially oxidized.* The shift to higher energy is the sum of two effects: the stabilization of the 1s level (as observed in photoelectron spectroscopy) and the destabilization of the 4p antibonding levels of the sulfur.

EXAFS analysis: A similar comparison is possible using the EXAFS tool. The qualitative comparison of the EXAFS signals (Figure 6) and Fourier transforms (Figure 7) of TTF, TTF-TCNQ, and $TTF(CoCl_4)_{0.28}$ allow us to conclude that the local environment around the sulfur in $TTF(CoCl_4)_{0.28}$ is closer to that in TTF-TCNQ than to that in neutral TTF.

The EXAFS results for TTF are in good agreement with crystallographic distances[18a,c] either within the molecule ($S–C_\alpha$ = 1.7415 ± 0.0185 Å, $S–C_\beta$ = 2.6184 ± 0.0067 Å) or between the molecules: the S–S intermolecular distance is found by EXAFS at 3.60 (2) Å (compared to 3.62 Å by XRD[18,b,c]). The mean number of sulfur neighbors of a given sulfur in a neutral TTF stack is 1.24. In the stacks of TTF^+ cations in TTF–TCNQ, this number is 2, because the molecular overlap for neutral molecules is less symmetrical than for cationic ones.[18c]

The first and second carbon shells in $TTF(CoCl_4)_{0.28}$ present no significant variation compared to TTF and TTF–TCNQ. However, the S–S intermolecular distance in $TTF(CoCl_4)_{0.28}$ is shorter (3.42 Å) than the one (3.60 Å) in TTF and closer to that (3.47 Å) in TTF-TCNQ. This short distance is consistent with a charge transfer along the TTF/TTF^+ stacks in $TTF(CoCl_4)_{0.28}$ as occurs in TTF-TCNQ. This S–S intermolecular distance is in agreement with those reported in the literature[6] and with preliminary XRD data[8c,d] which describe the organic lattice of $TTF(CoCl_4)_{0.28}$ as two sets of orthogonal nonequivalent triads in a crystallographic plane and two isolated TTF molecules laying in the (100) plane of the unit cell: the interplanar stacking distance is 3.38 Å in the symmetrical trimer and 3.30 and 3.31 Å in the unsymmetrical one. The average number of backscattering S atoms obtained by fitting as 1.33 is in agreement with the trimeric structure considered as a perfect stack along the orthogonal axis of the TTF ring.

The fourth peak of $TTF(CoCl_4)_{0.28}$ can be attributed to the $S_1–S_1'$ and $S_2–S_2'$ intramolecular distance as in TTF, to the S–S distance between TTF molecules of different kind of trimers (3.58, 3.67, 3.75, and 3.83 Å computed from XRD[8d]) and probably to S–Cl distances.

(2) BEDT-TTF Derivatives. XANES analysis: (i) The spectra of complexes prepared from BEDT-TTF and inorganic ions MCl_4^{2-} (M = Mn, Co, Zn) show a tetrahedral coordination around the metal as in the TTF series.

(ii) The copper compound, which has a metallic-like electrical conductivity is different from the other members of the series; it gives an entirely different X-ray absorption spectrum. Earlier studies of square planar copper[26] and iron[27] complexes have firmly established that the presence of a clear transition in the leading edge is characteristic of a square-planar structure. This band can be assigned to a z-polarized transition, to a $Cu(4p_z)$ state.

The weak intensity of the preedge in Figure 8C is related to the presence of an inversion center in the square-planar complex with Cu(II) d^9 configuration (dipole forbidden, quadrupole allowed transition).

EXAFS analysis: We have analyzed the first shell in the EXAFS spectrum of the $BEDT-TTF(MCl_4)_{0.3}$ compounds, where M = Mn, Co and Zn. On one hand, the agreement factor ρ is worse than in the TTF series, in particular for the manganese complex. On the other hand, for all compounds the Debye–Waller factor is higher than in the TTF series. The high values of the Debye–Waller factor characterize a larger distribution of the ligand distances around the metal than in $TTF(MCl_4)_{0.28}$.

We next attempted a two–shells fitting procedure to account for such a distribution of the metal-to-ligand distances: we have considered two different metal–chloride distances with 2+2 neighbors. We show these results for the cobalt complex in Table XII.

The Debye–Waller factor decreases by using the two-shell fitting procedure, and two Co–Cl distances are found, one smaller than the Co–Cl distance in the one-shell fit and the other larger. We conclude that a distribution of distances around the mean value obtained by the single-shell fit is likely. The data analysis does not allow us to specify the distribution: we have either two different distances within a unique but distorted tetrahedron or two regular tetrahedrons.

(3) $TTF(MnCl_3)_{0.75}$ Chain. XANES analysis: The comparison between the manganese K-edge spectra (Figure 9) of $TTF(MnCl_3)_{0.75}$ and of tetramethylammonium manganese trichloride, TMMC, which is the archetype of the one-dimensional antiferromagnetic systems, allow us to conclude that in both materials the metal is in a quasi-octahedral symmetry. The spectra at the chloride K edge (Figure 10) show nevertheless that the octahedrons do not have the same distortions. The absence of clear EXAFS oscillations in the spectrum of $TTF(MnCl_3)_{0.75}$ can be a result of destructive interference between phase functions in the EXAFS signal.

EXAFS analysis: The EXAFS quality of fit is worse than in the tetrahedral complexes. Indeed, we reach here the limit of the EXAFS technique. A preliminary account

Table XII. EXAFS Results at the Cobalt K Edge in $BEDT-TTF(CoCl_4)_{0.3}$: Comparison between Single-Shell and Two-Shells Fitting Procedure

$BEDT-TTF(CoCl_4)_{0.3}$	N_1	R_1, Å	N_2	R_2, Å	σ, Å	$\Gamma = k/\lambda$	ρ, %
one shell	4	2.26 (2)			0.086	0.45	0.7
two shells	2	2.34 (2)	2	2.20 (2)	0.038	0.51	0.6

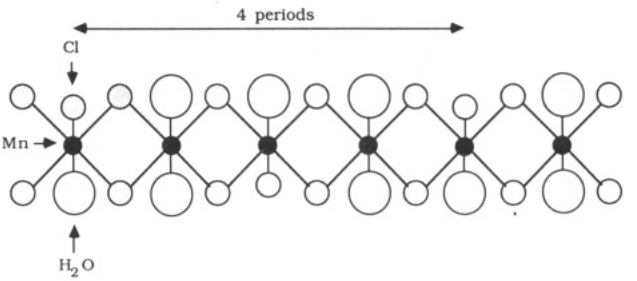

Figure 12. Schematic drawing of the room-temperature crystal structure of the manganese chain in $TTF(MnCl_3)_{0.75}$.[24]

(23) (a) Figgis, B. N.; Gerloch, M.; Mason, R. *Acta Crystallogr.* **1964**, *17*, 506. (b) Figgis, B. N.; Kucharski, E. S.; Reynolds, P. A. *Acta Crystallogr.* **1989**, *B45*, 232, 240.
(24) Gaultier, J., private communication.
(25) Fjaer, E. *Acta Crystallogr.* **1985**, *B41*, 330.
(26) Smith, T. A.; Penner-Hahn, J. E.; Berding, M. A.; Doniach, S.; Hodgson, K. O. *J. Am. Chem. Soc.* **1985**, *107*, 5945.
(27) Cartier, C.; Momenteau, M.; Dartyge, E.; Fontaine, A.; Tourillon, G.; Bianconi, A.; Verdaguer, M., *Biochimica Biophys. Acta*, in press.

(28) Available as supplementary material. See the paragraph at the end of the paper.

of a XRD structure in progress[8d] gives the key to the solution of the problem (Figure 12). The compound presents two different Mn centers along the chain: a $MnCl_4(H_2O)_2$ unit where Mn is at the center of an octahedron built from four Cl atoms in the basal plane and from two water molecules in apical position and a $MnCl_4Cl(H_2O)$ unit where a chlorine replaces one of the two water molecules in the preceding unit. The periodicity along the chain of these two units is 4 (Figure 12).

The results confirm the XANES analysis and demonstrate that EXAFS can give only an averaged structural solution.

Our three-shell fitting procedure gives results which agree with the preliminary XRD conclusions[8d] and confirms the existence of two kinds of manganese environments. The XRD distances are 2.46 and 2.54 Å for the Mn–Cl shells, and 2.08 and 2.30 Å for the Mn–O distances.

The distribution of distances for the Mn–Cl shells is given by the Debye–Waller factor, σ = 0.12 and 0.06 Å, respectively. We note the large Debye–Waller factor for the Mn–O shell (σ = 0.13 Å). This value is quite surprising because the Mn–O distance is shorter than the Mn–Cl distances. Indeed the values in Table VIII are to be analyzed with caution since, as we already said, we reach the limit of the EXAFS analysis (large number of parameters, weak contribution of oxygen atoms within the chlorine atoms signals, etc.).

At larger distances, as one expects in such a 1D structure, there is a Mn–Mn shell. The distance between the manganese centers is fitted at 3.28 Å. This value is of the same order of magnitude as the Mn–Mn distance reported in TMMC (3.247[19]).

Conclusion

The results of this extensive X-ray absorption fine structures (XAFS) study using synchrotron radiation allow us to show the interest and the limits of such a technique applied to the structural characterization of materials.

As for the limits, they are reached as in every absorption technique, when several different species belonging to the same absorber are present: the absorbance is the mean of the different signals and the conclusions may be drawn only about this mean. $TTF(MnCl_3)_{0.75}$ is such an example, even if it is rewarding that our structural analysis confirms the preliminary X-ray diffraction data. Furthermore, defects in the structures, which are known to be important in the determination of macroscopic properties, cannot be detected.

EXAFS allows us to determine the metal–chloride distances and the sulfur–neighbors distances in systems for which no single crystals are available, with an accuracy of ≈0.02 Å. In the present case, we determine all the M–Cl distances and we were able to check their accuracy in the few cases where XRD data were available. No indication of close neighbors beyond the first chlorine coordination sphere is detected. Hence, the MX_4 anions appear structurally insulated. Their charge and their geometries induce a given stacking of the organic moiety only through weak intermolecular contacts. At the sulfur edge, it is possible to distinguish clearly between the packing of unoxidized and oxidized stacks of TTF molecules: the decrease of the intermolecular S–S distances appears as a structural fingerprint of the semiconducting systems.

XANES allows us to specify the stereochemistry around the heavy atoms, when the physical properties (here conductivity) preclude the usual electronic sepctroscopic characterization in the visible and ultraviolet range. Here XANES reveals the similarity of the geometry of the Mn, Co, Zn counterions in the TTF and BEDT-TTF salts as distorted tetrahedral species. Instead, the copper-containing counterion is found in a square-planar geometry. No long-range structural information can be extracted from this local structure but the square-planar $CuCl_4^{2-}$ complex induces a particular and conducting stacking of the BEDT-TTF molecules, not found with the tetrahedral anions.

XANES also gives insights into the electronic structure of the absorbing atoms: as expected, the studied metallic ions present edge characteristics of bivalent metallic ions, whereas the chlorine K edges are in line with chloride species. Hence there is no evident electronic interactions between the inorganic anions and organic entities in the semiconducting materials, whatever the nature of the metallic ion may be. The main role of inorganic counterions is to insure the electronic charge balance in the system. More interesting is the observation of the *local oxidation* at the sulfur atom in the partially oxidized TTF molecules revealed by the significant shift to higher energy of the sulfur "white line". This appears as a clear electronic fingerprint of the charge-transfer process.

Acknowledgment. We acknowledge the help of J. P. Renard for a generous gift of TMMC crystals and of J. Gaultier for communication of unpublished X-ray diffraction data.

Registry No. $TTF(MnCl_3)_{0.28}$, 109144-01-6; $TTF(CoCl_3)_{0.28}$, 109144-03-8; $TTF(ZnCl_4)_{0.28}$, 118153-94-9; $BEDT\text{-}TTF(MnCl_3)_{0.3}$, 113803-79-5; $BEDT\text{-}TTF(CoCl_4)_{0.3}$, 113814-10-1; $BEDT\text{-}TTF(ZnCl_4)_{0.3}$, 113803-83-1; $BEDT\text{-}TTF(CuCl_4)_{0.3}$, 113803-81-9; $TTF(MnCl_3)_{0.75}$, 99553-13-6; S, 7704-34-9; Cl, 7782-50-5; Mn, 7439-96-5; Co, 7440-48-4; Zn, 7440-66-6; Cu, 7440-50-8.

Supplementary Material Available: Figures S1–S10 presenting the experimental data and analysis as quoted in the text (11 pages). Ordering information is given on any current masthead page.